Noninvasive Intracranial Pressure Assessment Based on a Data-Mining Approach Using a Nonlinear Mapping Function

Sunghan Kim, Fabien Scalzo, Marvin Bergsneider, Paul Vespa, Neil Martin, and Xiao Hu*

***Abstract*—The current gold standard to determine intracranial pressure (ICP) involves an invasive procedure for direct access to the intracranial compartment. The risks associated with this invasive procedure include intracerebral hemorrhage, infection, and discomfort. We previously proposed an innovative data-mining framework of noninvasive ICP (NICP) assessment. The performance of the proposed framework relies on designing a good mapping function. We attempt to achieve performance gain by adopting various linear and nonlinear mapping functions. Our results demonstrate that a nonlinear mapping function based on the kernel spectral regression technique significantly improves the performance of the proposed data-mining framework for NICP assessment in comparison to other linear mapping functions.**

***Index Terms*—Data mining, kernel spectral regression (KSR), noninvasive ICP (NICP), nonlinear mapping function, ordinary least squares (OLS), quadratic programming (QP), recursive weighted least squares (RWL).**

I. Introduction

An accurate determination of intracranial pressure (ICP) is valuable for the diagnosis and/or management of a wide variety of neurological disorders. The current gold standard involves an invasive procedure (surgical penetration of the skull) for direct access to the intracranial compartment. The risks associated with this invasive procedure include intracerebral hemorrhage, infection, and discomfort. They may obviate its application in many clinical circumstances. There are several clinical situations in which an assessment of ICP is desirable but an invasive procedure is contraindicated. These situations include management of patients with fulminant hepatic failure [1], [2] and pregnant women with preeclampsia [3]. A reliable noninvasive ICP (NICP) assessment procedure could alter the current treatment and management protocols for those patients.

The following scenarios exemplify the potential utility of an NICP assessment technique in improving the care and management of patients with complex problems. First, it is often difficult to determine whether the shunt is working properly in the follow-up management of hydrocephalus patients with implanted shunts. An NICP protocol would be less costly and safer to address this need in an outpatient setting than implanting an invasive telemetric ICP device. Second, several studies have shown that elevated ICP is associated with an unfavorable outcome for liver transplant recipients [4], [5]. However, patients with liver disease often suffer from coagulopathy (bleeding disorder) and the risks of invasive ICP monitoring in patients with coagulopathy overshadow the benefits of predicting outcome [1]. In contrast, an NICP assessment procedure could be safely and easily applied. Therefore, it could aid clinical decision making in the selection of patients with fulminant hepatic failure for liver transplantation. In the United States alone there are around 6500 liver transplant cases annually while 8% of those are for treatment of fulminant hepatic failure. Third, the NICP assessment would provide valuable information in traumatic brain injury (TBI) patients during interhospital emergency transfer from smaller hospitals to major trauma or neurosurgical centers or can be used in battle field for safe triage of injured warriors.

Several groups have attempted to develop NICP assessment techniques during the last decade. However, none of those techniques has proved significant clinical applicability. Each technique has problems in order to be accepted into wide clinical practice. For example, the ultrasound-based apparatus cannot provide absolute values of ICP because of the lack of a defined mathematical relationship between the measured physiologic variable and ICP [6], [7]. The tissue resonance analysis, which measures the transfer time of cerebral arterial blood to cerebral venus blood to infer ICP using an empirical linear mapping function, is technically complex and lacks a method to quantify the goodness of inference [8]. Transcranial Doppler (TCD) can noninvasively measure cerebral blood flow velocity (CBFV) at major cerebral basilar arteries and three empirical formulas have been proposed for relating arterial blood pressure (ABP) and CBFV to cerebral perfusion pressure. However,

Manuscript received June 14, 2010; revised November 1, 2010; accepted November 3, 2010. Date of publication November 22, 2010; date of current version February 17, 2012. *Asterisk indicates corresponding author*.

S. Kim and F. Scalzo are with the Neural Systems and Dynamics Laboratory, Department of Neurosurgery, David Geffen School of Medicine at University of California, Los Angeles, CA 90095-7065 USA (e-mail: visionsk@gmail.com; fscalzo@mednet.ucla.edu).

M. Bergsneider is with the UCLA Adult Hydrocephalus Center, Department of Neurosurgery, David Geffen School of Medicine at University of California, Los Angeles, CA 90095-7065 USA (e-mail: mbergsneider@mednet.ucla.edu).

P. Vespa is with the Neurocritical Care Program, Department of Neurosurgery, David Geffen School of Medicine at University of California, Los Angeles, CA 90095-7065 USA (e-mail: pvespa@mednet.ucla.edu).

N. Martin is with the UCLA Stroke Center, Department of Neurosurgery, David Geffen School of Medicine at University of California, Los Angeles, CA 90095-7065 USA (e-mail: nmartin@mednet.ucla.edu).

*X. Hu is with the Neural Systems and Dynamics Laboratory, Department of Neurosurgery, David Geffen School of Medicine at University of California, Los Angeles, CA 90095-7065 USA (e-mail: xhu@mednet.ucla.edu).

Color versions of one or more of the figures in this paper are available online at http://ieeexplore.ieee.org.

Digital Object Identifier 10.1109/TBME.2010.2093897

none of these formula-based methods is capable of assessing ICP waveform and quantifying the quality of the resultant estimate [9]–[11]. A more advanced TCD-based approach proposed by Schmidt *et al*.s capable of estimating actual ICP waveform by inputting ABP and CBFV to an ICP simulation model [12], [13]. Since the model is identified by processing a collection of ABP, CBFV, and invasive ICP signals, this approach can be thought of as a preliminary form of a data-mining method. Two major weaknesses of the approach are its rigid structure, which prevents it from being readily converted to a modular method, and the incapability of assessing the quality of the resultant estimate.

We previously proposed an innovative data-mining framework of NICP assessment in [14]. The proposed data-mining framework explores the rules of deriving ICP from ABP and CBFV that are captured implicitly by a signal database without using an explicit first-principle driven mathematical model. This approach is particularly attractive for our scenario where an accurate mathematical model of ABP, CBFV, and ICP is challenging to build and its parametrization based on clinically available measurements is extremely difficult if not impossible. Another advantage of the proposed data-mining framework is that it can be presented as a general time series estimation technique with a case-based reasoning paradigm [15]. Estimating aorta pressure (*target time series*) from blood pressure signals of multiple peripheral sites (*related time series*) is one example of applying the proposed data-mining framework as the general time series estimation technique. The NICP assessment is a special case of the general time series estimation technique where the *target time series* is ICP and the *related time series* are ABP and CBFV.

The main strategy of the proposed framework is to provide a *mapping function* to quantify the uncertainty of an ICP estimate associated with each database entry and to use this information to determine the best entry to build an ICP simulation model, which can be used to obtain an optimal ICP estimate. Designing a good mapping function, therefore, is essential for the reliable performance of the proposed data-mining framework. Our first choice of the mapping function was a simple ordinary least squares (OLS). Although our data-mining framework with the OLS linear mapping function outperformed existing data-mining techniques for NICP assessment [14], [15], the performance of NICP assessment has not reached a satisfactory level for our data-mining framework to be accepted into routine use in neurosurgical services. The main objectives of the current work are to adopt new (linear and nonlinear) mapping functions into our data-mining framework for NICP estimation and demonstrate that the performance of NICP assessment can be improved by utilizing proper mapping functions.

II. Methodology

A. Data-Mining Framework

This section provides a brief introduction of our data-mining approach to NICP assessment for better understanding of the current study. The complete description of the data-mining framework should be referred to our previous publications [14], [15].

Our data-mining framework exploits a database of simultaneously recorded signals (ABP, CBFV, and ICP) and dynamic models of the signals (inputs: ABP and CBFV, output:ICP). Two types of important data are drawn from this database: *hemodynamic features* and *dissimilarity measures*. Hemodynamic features are extracted from ABP and CBFV to capture the characteristic aspects of the cerebral hemodynamic state. These hemodynamic features contain information about ICP because the cerebral hemodynamics is under the influence of the cerebral spinal fluid dynamics [16], [17]. Dissimilarity measures are calculated as the distance between true ICP and its estimates, which can be obtained by simulating the dynamic models in the database. In other words, dissimilarity measures quantify how closely each dynamic model can estimate true ICP only given corresponding ABP/CBFV signals. Then, the main strategy of the data-mining framework is to formulate a *mapping function* between hemodynamic features and dissimilarity measures. In other words, the mapping function needs to be *trained* to estimate dissimilarity measures given hemodynamic features. When ABP and CBFV signals are collected from a new patient whose ICP is unknown, the mapping function takes hemodynamic features extracted from his/her ABP and CBFV signals as its input and outputs the estimated dissimilarity measures of all dynamic models. These estimated dissimilarity measures are used to identify the most appropriate dynamic model among all dynamic models. By simulating the identified dynamic model with the patient's ABP and CBFV signals, one can obtain an estimate of his/her unknown true ICP.

We used a linear dynamic system (LDS) to model the relation between ABP, CBFV, and ICP signals. Considering the complex nonlinear characteristics of ICP dynamics, one may wonder whether the LDS model is an appropriate form to model the relation between ABP, CBFV, and ICP signals. However, our recent systematic study of the LDS model's data fitting capability and generalizability indicated that the LDS model is a plausible choice to model the complex nonlinear ICP dynamics for a short period of recordings, which was 100 heartbeat long in all our previous studies. This study result is under review for publication at Physiological Measurement.

Current hemodynamic features are the coefficients of a linear autoregressive with exogenous input (ARX) model that fits the ABP(input)/CBFV(output) signals. Although more complex nonlinear models can be used, Panerai *et al*. emonstrated that a LDS is adequate to model dynamic cerebral autoregulation [17]. More details about the hemodynamic feature selection process can be found in [14] and [18].

Dissimilarity measures, i.e., the distance between true ICP and its estimates, can be defined in many ways since ICP signals reflect various physiological and pathophysiological conditions of the intracranial system. In [14], we defined five types of *dissimilarity measures* that concern the most relevant aspects of routine ICP monitoring. In the current study, we will stay focused on three dissimilarity measures that are closely related to mean ICP ($\overline{\text{ICP}}$) and correlation between normalized ICP

signals. They can be expressed as follows:

$$e^{(2)} = \frac{|\overline{\text{ICP}} - \overline{\widehat{\text{ICP}}}|}{|\overline{\text{ICP}}|} \tag{1}$$

$$e^{(3)} = 1 - \text{corr}(\text{ICP}^N, \widehat{\text{ICP}}^N) \tag{2}$$

$$e^{(5)} = \frac{1}{N} \frac{\sum_{i=1}^{N} |\text{ICP}_i^S - \widehat{\text{ICP}}_i^S|}{\|\text{ICP}^S\|} \tag{3}$$

where ICP_i is the ith sample of an original (true) ICP signal, $\widehat{\text{ICP}}_i$ its corresponding estimate, $\overline{\text{ICP}}$ its mean, ICP^N the normalized ICP, and ICP^S the slow wave component of ICP. We normalized ICP by its mean so that $\text{ICP}^N = (\text{ICP} - \overline{\text{ICP}})/\overline{\text{ICP}}$.

B. Mapping Functions

Our first choice of mapping function was an OLS, which is a linear regression technique [14], [15]. In the current study, we introduce three more mapping functions utilizing two linear and one nonlinear techniques.

1) Ordinary Least Squares (OLS or L1): The OLS was our first choice of mapping function due to its simplicity and ease of implementation. Let us suppose that F represents a hemodynamic feature matrix and E a dissimilarity measure matrix. The jth column of the hemodynamic feature matrix F is the hemodynamic feature vector (ARX model coefficients) of the jth entry. On the other hand, the dissimilarity measure $E(i,j)$, i.e., the ith-row and jth-column element of E, quantifies how closely the true ICP of the jth entry can be estimated by simulating the dynamic model of the ith entry with ABP/CBFV signals of the jth entry. Then, the OLS mapping matrix B can be obtained as follows:

$$E = B^{\mathrm{T}} F \tag{4}$$

$$\hat{B} = \left(FF^{\mathrm{T}}\right)^{-1} FE^{\mathrm{T}} \tag{5}$$

where E is an $N_{\mathrm{e}} \times N_{\mathrm{e}}$ dissimilarity measure matrix, F a $d \times N_{\mathrm{e}}$ hemodynamic feature matrix, B a $d \times N_{\mathrm{e}}$ mapping matrix, N_{e} the number of entries, and d the dimension of the hemodynamic feature vector, i.e., the number of hemodynamic features. When a hemodynamic feature vector f_{new} is extracted from ABP and CBFV signals of a new patient, the dissimilarity measure vector $\hat{e}$ is estimated as follows:

$$\hat{e}_{\mathrm{new}} = \hat{B}^{\mathrm{T}} f_{\mathrm{new}} \tag{6}$$

where $\hat{e}_{\mathrm{new}}$ is an $N_{\mathrm{e}} \times 1$ dissimilarity measure vector and f_{new} a $d \times 1$ hemodynamic feature vector.

2) Recursive Weighted Least Squares (RWL or L2): The OLS mapping function described earlier is based on a *multivariate* regression technique since the number of variables to estimate is greater than 1. In fact, the total number of variables to estimate is N_{e} since $\hat{e}_{\mathrm{new}}$ in (6) is an $N_{\mathrm{e}} \times 1$ vector. The multivariate regression expressed in (4)–(6) can be thought of as a combination of multiple single-variate regressions. A single-variate regression can be expressed as follows:

$$E(i,:) = B(:,i)^{\mathrm{T}} F \tag{7}$$

Algorithm 1 Recursive Weighted Least Squares

$W_1 = I$
for $n = 1, ..., N_{\mathrm{t}}$ **do**
  $E = EW_n$ & $F = FW_n$
  $\hat{B} = \left(FF^{\mathrm{T}}\right)^{-1} FE^{\mathrm{T}}$
  $\hat{E} = \hat{B}^{\mathrm{T}} F$
  for $j = 1, ..., N_{\mathrm{e}}$ **do**
    $\omega_n(j) = \|E(:,j) - \hat{E}(:,j)\|$
  end for
  $\omega_n = \frac{\omega_n}{\max(\omega_n)}$
  $\text{diag}\,(W_n) = \omega_n$
end for

where I is a $N_{\mathrm{e}} \times N_{\mathrm{e}}$ identity matrix, W a $N_{\mathrm{e}} \times N_{\mathrm{e}}$ weighting matrix, N_{t} the number of iterations, and $\text{diag}\,(W)$ diagonal elements of W.

$$\hat{B}(:,i) = \left(FF^{\mathrm{T}}\right)^{-1} FE(i,:)^{\mathrm{T}} \tag{8}$$

$$\hat{e}_{\mathrm{new}}(i) = \hat{B}(:,i)^{\mathrm{T}} f_{\mathrm{new}} \tag{9}$$

where $\hat{e}_{\mathrm{new}}(i)$ is estimated solely based on the corresponding row vector $E(i,:)$. In other words, the OLS mapping function based on the canonical multivariate regression does not utilize any *column-wise* relations of the elements of E. The RWL was devised as an attempt to overcome the limitation of the canonical multivariate regression technique. The RWL performs the weighted least squares *recursively* by updating the weighting matrix W at each iteration. Algorithm 1 describes the details of the RWL mapping function. Briefly, the jth element of the weighting vector ω, i.e., $\omega(j)$, is proportion to $\|E(:,j) - \hat{E}(:,j)\|$, which is the norm of the *column-wise* estimation error of E. The elements of ω become the diagonal elements of the weighting matrix W. The rationale for this weighting scheme is to reduce the variance of ω after each iteration so that eventually the column-wise estimation errors of E become somewhat uniform.

3) Quadratic Programming with Constraints (QP or L3): The QP is an optimization method to minimize or maximize a quadratic function of unknown parameters with additional linear constraints (inequality and/or equality) [19]. The linear least-squares problem can be framed as an optimization problem whose objective function can be expressed as a quadratic function of b_i as follows:

$$\begin{aligned}\mathcal{O}\left(B(:,i)\right) &= \|E(i,:) - B(:,i)^{\mathrm{T}} F\|^2 \qquad (10)\\ &= E(i,:)E(i,:)^{\mathrm{T}} - 2E(i,:)F^{\mathrm{T}} B(:,i)\\ &\quad + B(:,i)^{\mathrm{T}} FF^{\mathrm{T}} B(:,i) \qquad (11)\end{aligned}$$

$$\hat{B}(:,i) = \underset{B(:,i)}{\arg\min}\left(\mathcal{O}\left(B(:,i)\right)\right) \tag{12}$$

where $\hat{b}_i$ is identical to the linear least-squares solution in (8). However, the QP enables us to impose additional linear constraints to the objective function in (11). They can be expressed as follows:

$$B(:,i)^{\mathrm{T}} F(:,j) \begin{cases} \leq \max\left(E(:^{-i},j)\right) & j = i \\ \geq \min\left(E(:^{-i},j)\right) & j \neq i \end{cases} \tag{13}$$

where $E(:^{-i},j)$ is the jth column vector of E excluding its ith element. The rationale behind the inequality constraints in (13)

is that the diagonal component $E(j,j)$ of the dissimilarity measure matrix E is supposed to have the smallest value among all elements of the corresponding column vector $E(:,j)$ because $E(j,j)$ is the distance between the jth entry's true ICP and its estimate by simulating its own dynamic model. Imposing the inequality constraints to the objective function $\mathcal{O}\left(B(:,i)\right)$ is another way to overcome the limitation of the canonical multivariate regression technique, which is not capable of incorporating any *column-wise* relations of the elements of E.

4) Kernel Spectral Regression (KSR or N): KSR [20] is a recently proposed method to solve kernel discriminant analysis problems efficiently. Specifically, it casts discriminant analysis into a regularized regression problem that exploits a spectral graph representation. It was successfully used in a wide variety of problems, such as face and digits recognition [20], and more recently for detecting peaks in ICP signals [21].

KSR captures nonlinearity through a kernel projection of the data. In this study, feature vectors F are projected onto a high-dimensional space via a Gaussian kernel K, defined as

$$K(i,j) = \mathrm{e}^{-\|F(:,i)-F(:,j)\|^2/2\sigma^2} \tag{14}$$

where σ is the user-specified standard deviation of the kernel.

Given known dissimilarity measures E, KSR estimates the mapping function B efficiently using a Cholesky decomposition as follows:

$$E = B^{\mathrm{T}}(K + \delta I) \tag{15}$$

$$E = B^{\mathrm{T}} L L^{\mathrm{T}} \tag{16}$$

where I is the identity matrix, $\delta \geq 0$ the regularization parameter, and L the lower triangular matrix.

When a new hemodynamic feature vector f_{new} is extracted from ABP and CBFV signal of a new patient, the dissimilarity measure vector $\hat{e}$ is estimated as follows:

$$k(i) = \mathrm{e}^{-\|F(:,i)-f_{\mathrm{new}}\|^2/2\sigma^2} \tag{17}$$

$$\hat{e} = \hat{B}^{\mathrm{T}}(k + \delta I) \tag{18}$$

where k is an $N_{\mathrm{e}} \times 1$ vector resulting from the kernel projection of f_{new} into the kernel space.

C. Experimental Design

The main concern of our experiments was to study whether the performance of the data-mining framework can be improved by adopting different mapping functions other than the previously proposed OLS mapping function. We were particularly interested in whether the nonlinear mapping function (KSR) is significantly better than the other linear mapping functions.

We analyzed the performance of the data-mining framework with different mapping functions from two perspectives. First, we compared the dissimilarity measure estimates, which are the distance between true ICP and its *best* estimate obtained by the data-mining framework. Depending on the type of dissimilarity measure, the distance between true ICP and its *best* estimate can be calculated as described in (1)–(3). Since our best concern was to investigate whether or not the KSR mapping function is superior to the other linear mapping functions, we reported the difference between the dissimilarity measure estimates as follows:

$$\Delta^{(\cdot)}_{\mathrm{N-L1}}(i) = e^{(\cdot)}_{\mathrm{N}}(i) - e^{(\cdot)}_{\mathrm{L1}}(i) \tag{19}$$

$$\Delta^{(\cdot)}_{\mathrm{N-L2}}(i) = e^{(\cdot)}_{\mathrm{N}}(i) - e^{(\cdot)}_{\mathrm{L2}}(i) \tag{20}$$

$$\Delta^{(\cdot)}_{\mathrm{N-L3}}(i) = e^{(\cdot)}_{\mathrm{N}}(i) - e^{(\cdot)}_{\mathrm{L3}}(i) \tag{21}$$

where the subscript N is for the KSR, the subscript L1 for the OLS, the subscript L2 for the RWL, and the subscript L3 for the QP. For example, $\Delta^{(2)}_{\mathrm{N-L1}}(i)$ is the difference between the ith entry's dissimilarity measure estimate of the KSR mapping function and that of the OLS mapping function, where the choice of dissimilarity measure is $e^{(2)}$. If $\Delta^{(2)}_{\mathrm{N-L1}}(i)$ has a negative value, it indicates that the KSR is a better choice than the OLS as the mapping function when the choice of dissimilarity measure is $e^{(2)}$. We present the difference Δ, both in the qualitative (graphical) and quantitative ways.

The dissimilarity measures were originally proposed to investigate particular aspects of NICP assessment in a *normalized* way [14]. For example, $e^{(3)}$ ranges between 0 and 2 where 0 represents a perfect positive correlation and 2 a perfect negative correlation. These normalized dissimilarity measures may be preferable for the purpose of the numerical performance analysis of the data-mining framework. However, clinicians may find it difficult to make much sense out of the numerical performance analysis results based on the normalized dissimilarity measures. They would rather be interested in clinically meaningful performance measures such as mean ICP estimation errors. Therefore, we report the absolute mean ICP estimation errors $\xi_{\cdot}(i)$(mmHg), which can be expressed as follow:

$$\xi_{\mathrm{L1}}(i) = |\overline{\mathrm{ICP}}^S_{\mathrm{T}}(i) - \overline{\mathrm{ICP}}^S_{\mathrm{L1}}(i)| \tag{22}$$

$$\xi_{\mathrm{L2}}(i) = |\overline{\mathrm{ICP}}^S_{\mathrm{T}}(i) - \overline{\mathrm{ICP}}^S_{\mathrm{L2}}(i)| \tag{23}$$

$$\xi_{\mathrm{L3}}(i) = |\overline{\mathrm{ICP}}^S_{\mathrm{T}}(i) - \overline{\mathrm{ICP}}^S_{\mathrm{L3}}(i)| \tag{24}$$

$$\xi_{\mathrm{N}}(i) = |\overline{\mathrm{ICP}}^S_{\mathrm{T}}(i) - \overline{\mathrm{ICP}}^S_{\mathrm{N}}(i)| \tag{25}$$

where $\overline{\mathrm{ICP}}^S_{\mathrm{T}}$ represents the true mean ICP of the slow component and $\overline{\mathrm{ICP}}^S_{\mathrm{L1}}$, $\overline{\mathrm{ICP}}^S_{\mathrm{L2}}$, $\overline{\mathrm{ICP}}^S_{\mathrm{L3}}$, and $\overline{\mathrm{ICP}}^S_{\mathrm{N}}$ represent the mean ICP estimates using the OLS mapping function, the RWL mapping function, the QP mapping function, and the KSR mapping function, respectively. We summarized the performance analysis results of mean ICP estimation by reporting four different percentiles (10th, 25th, 50th, and 75th) of ξ_{L1}, ξ_{L2}, ξ_{L3}, and ξ_{N}. In order to visualize the performance difference between the KSR and three other linear mapping functions, we also plotted the difference between the absolute mean ICP estimation errors, i.e., $\xi_{\mathrm{N}}(i) - \xi_{\mathrm{L1}}(i)$, $\xi_{\mathrm{N}}(i) - \xi_{\mathrm{L2}}(i)$, and $\xi_{\mathrm{N}}(i) - \xi_{\mathrm{L3}}(i)$.

The performance of the data-mining framework with different mapping functions was validated based on the leave-one-patient-out schema as in [22] and [14]. In other words, a mapping function is trained using the entries from all but one patient and tested on the remaining one.

III. Data Collection

We collected ICP, ABP, CBFV at the middle cerebral arteries (MCAs), and ECG from 57 head-injured patients (ages: 18–89 [median: 47], gender: 42 males/15 females). They were admitted to Ronald Reagan UCLA Medical Center between July 15, 2008 and November 16, 2009. Among them, 31 patients had TBI, 20 subarachnoid hemorrhage (SAH), 3 intracranial hemorrhage, 2 intracerebral hemorrhage, and 1 hydrocephalus.

The signals were collected while technicians affiliated with the Cerebral Blood Flow (CBF) laboratory at UCLA Department of Neurosurgery conducted daily clinical assessment of patients' cerebral hemodynamics using TCD, which involves the insonation of multiple intracranial arteries. The duration of collected signals varies depending on how long the TCD monitoring of the MCAs could be done. Typically, the TCD monitoring lasted only 3–5 min when the probe had to be handheld or 10–20 min when the probe was fixed to a headband around the patient's head. All signals were acquired through an analog connection from the bedside monitor to a 16-port amplifier from ADInstrument and were sampled at 400 Hz. The total recording length of all signals from 57 patients was approximately 8 h. The total number of entries was 382 where each entry included only the 100 heartbeat time period of the simultaneous recorded ABP, CBFV, and ICP signals. It should be noted that each entry's signal length in the unit of seconds varies depending on the corresponding heart rate. This signal length (100 heartbeat time period) was chosen so that the signal's long-term characteristics can be captured properly and yet its dynamic system is assumed to remain stable [14].

This study was approved by Institutional Review Board (IRB) as a data analysis project without involvement of any personal health information.

IV. Results

A. Dissimilarity Measure Estimation

Three plots in Fig. 1 depict the difference between the dissimilarity measure estimates: $\Delta^{(2)}_{\mathrm{N-L1}}(i)$ (top), $\Delta^{(2)}_{\mathrm{N-L2}}(i)$ (middle), and $\Delta^{(2)}_{\mathrm{N-L3}}(i)$ (bottom), respectively. It is obvious that $\Delta^{(2)}_{\mathrm{N-L1}}(i)$, $\Delta^{(2)}_{\mathrm{N-L2}}(i)$, and $\Delta^{(2)}_{\mathrm{N-L3}}(i)$ have negative values for most entries (≈85%). The first row of Table I confirms that on average $\Delta^{(2)}_{\mathrm{N-L1}}(i)$, $\Delta^{(2)}_{\mathrm{N-L2}}(i)$, and $\Delta^{(2)}_{\mathrm{N-L3}}(i)$ are smaller than zero. It is convincing that the KSR mapping function is superior to three other linear mapping functions in terms of estimating the dissimilarity measure $e^{(2)}$.

Three plots in Fig. 2 illustrate the difference between the dissimilarity measure estimates: $\Delta^{(3)}_{\mathrm{N-L1}}(i)$ (top), $\Delta^{(3)}_{\mathrm{N-L2}}(i)$ (middle), and $\Delta^{(3)}_{\mathrm{N-L3}}(i)$ (bottom), respectively. Although three plots show that $\Delta^{(3)}_{\mathrm{N-L1}}(i)$, $\Delta^{(3)}_{\mathrm{N-L2}}(i)$, and $\Delta^{(3)}_{\mathrm{N-L3}}(i)$ have negative values for the majority of entries (≈90%), on average they are just slightly smaller than zero as listed on the second row of Table I. One may argue that ave$(\Delta^{(3)}_{\mathrm{N-L1}})$, which is -0.07, may not be significantly different from 0 in a statistical sense. So, we performed the Friedman test to determine whether $\Delta^{(3)}_{\mathrm{N-L1}}(i)$ is significantly different from 0. The p-value of the Friedman test was very close to 0, which indicates that $\Delta^{(3)}_{\mathrm{N-L1}}$ is significantly smaller than 0 in a statistical sense although its mean value is only -0.07. The same conclusion could be drawn for ave$(\Delta^{(3)}_{\mathrm{N-L2}})$ and ave$(\Delta^{(3)}_{\mathrm{N-L3}})$. Therefore, it is plausible to argue that the KSR mapping function is a better choice than the other linear mapping functions in terms of estimating the dissimilarity measure $e^{(3)}$.

Three plots in Fig. 3 show the difference between the dissimilarity measure estimates: $\Delta^{(5)}_{\mathrm{N-L1}}(i)$ (top), $\Delta^{(5)}_{\mathrm{N-L2}}(i)$ (middle),

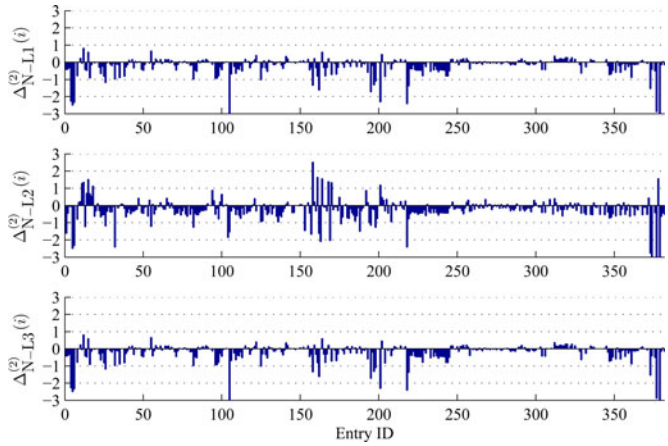

Fig. 1. Difference between the dissimilarity measure $e^{(2)}$ estimates: KSR versus OLS(L1) (top), KSR versus RWL(L2) (middle), and KSR versus QP(L3) (bottom). Each bar becomes negative when the KSR mapping function outperforms the linear mapping functions.

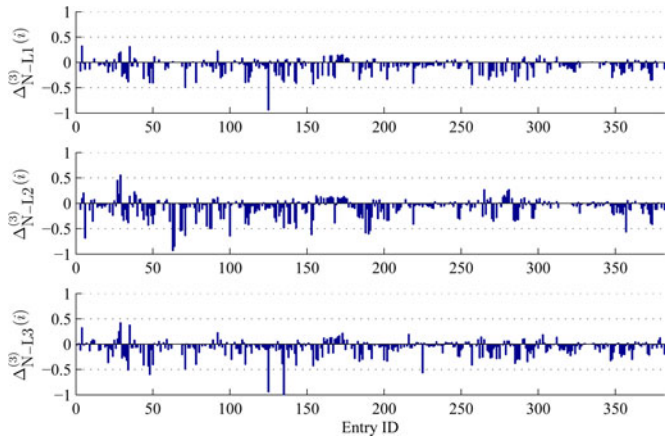

Fig. 2. Difference between the dissimilarity measure $e^{(3)}$ estimates: KSR versus OLS(L1) (top), KSR versus RWL(L2) (middle), and KSR versus QP(L3) (bottom). Each bar becomes negative when the KSR mapping function outperforms the linear mapping functions.

TABLE I
SUMMARY OF THE AVERAGE VALUES OF THE DISSIMILARITY DIFFERENCES

Error Type	ave$(\Delta^{(\cdot)}_{\mathrm{N-L1}})$	ave$(\Delta^{(\cdot)}_{\mathrm{N-L2}})$	ave$(\Delta^{(\cdot)}_{\mathrm{N-L3}})$
$e^{(2)}$	-0.21	-0.26	-0.20
$e^{(3)}$	-0.07	-0.08	-0.06
$e^{(5)}$	-0.15	-0.13	-0.14

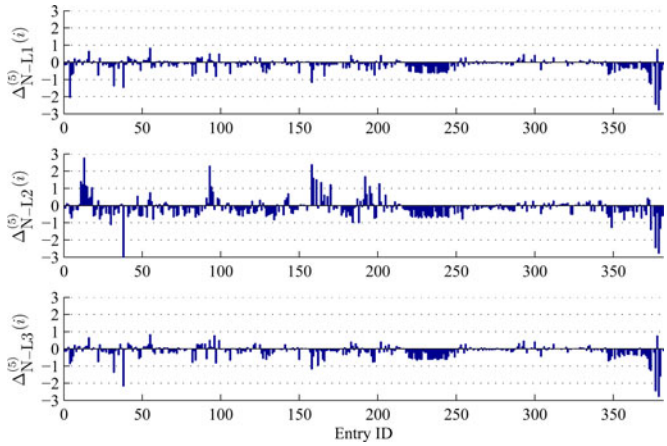

Fig. 3. Difference between the dissimilarity measure $e^{(5)}$ estimates: KSR versus OLS(L1) (top), KSR versus RWL(L2) (middle), and KSR versus QP(L3) (bottom). Each bar becomes negative when the KSR mapping function outperforms the linear mapping functions.

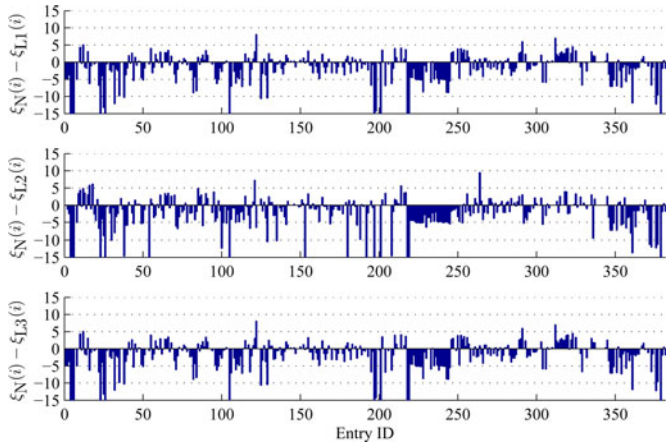

Fig. 4. Difference between the absolute mean ICP estimation errors $\xi_{\cdot}(i)$: KSR versus OLS(L1) (top), KSR versus RWL(L2) (middle), and KSR versus QP(L3) (bottom). Each bar becomes negative when the KSR mapping function estimates the true mean ICP more accurately than the linear mapping functions.

TABLE II
SUMMARY OF THE PERCENTILES OF THE MEAN ICP ESTIMATION ERRORS ($\xi_{\cdot}$) IN mmHg

Percentiles	ξ_{L1}	ξ_{L2}	ξ_{L3}	ξ_{N}
10	1.38	1.39	1.38	0.35
25	3.35	3.64	3.36	1.37
50	**5.63**	**6.07**	**5.63**	**4.37**
75	9.57	10.04	9.58	7.58

and $\Delta^{(5)}_{\mathrm{N-L3}}(i)$ (bottom), respectively. The third row of Table I lists ave($\Delta^{(5)}_{\mathrm{N-L1}}$), ave($\Delta^{(5)}_{\mathrm{N-L2}}$), and ave($\Delta^{(5)}_{\mathrm{N-L3}}$), which are definitely smaller than 0. Therefore, the KSR mapping function is believed to surpass the other linear mapping functions in terms of estimating the dissimilarity measure $e^{(5)}$.

B. Mean ICP Estimation

Each column of Table II summarizes four different percentiles of the absolute mean ICP estimation errors $\xi_{\cdot}$ of each mapping function. It is important to notice that the percentile values of ξ_{N} (fourth column) are noticeably smaller than those of the others, i.e., ξ_{L1}, ξ_{L2}, and ξ_{L3}. Especially, the 50th percentile (median) of ξ_{N} is as small as 4.37 mmHg while those of the others are greater than 5.6 mmHg. We performed the Friedman test to examine whether ξ_{N} is significantly different from each of ξ_{L1}, ξ_{L2}, and ξ_{L3} in a statistical sense. The *p*-values of three Friedman tests between ξ_{N} and ξ_{L1}, ξ_{N} and ξ_{L2}, and ξ_{N} and ξ_{L3} were virtually 0, which indicate that the KSR mapping function yielded significantly smaller absolute mean ICP estimation errors than the other linear mapping functions. Three plots in Fig. 4 visualize the differences between the absolute mean ICP estimation errors, $\xi_{\mathrm{N}}(i)-\xi_{\mathrm{L1}}(i)$ (top), $\xi_{\mathrm{N}}(i)-\xi_{\mathrm{L2}}(i)$ (middle), and $\xi_{\mathrm{N}}(i)-\xi_{\mathrm{L3}}(i)$ (bottom), respectively. In all three plots, it is obvious that the differences are smaller than 0 for most entries (87%).

V. DISCUSSIONS AND CONCLUSION

A. Query Method

A mapping function takes a hemodynamic feature vector f as its input and outputs an estimated dissimilarity measure vector $\hat{e}$. Based on this estimated dissimilarity measure vector, then, a query engine selects the best entry in the database according to a certain criterion. In [14], we investigated two distinct query methods: a deterministic and statistical query. In short, the deterministic query returns the database entry with the smallest estimated dissimilarity measure while the statistical query returns the database entry with the largest z-test score. The study results showed that the statistical query method was preferable over the deterministic one in terms of its robustness to some erroneous entries [14]. In the current study, however, we implemented the deterministic query method instead of the statistical one. The main reason was that the statistical query method requires the computation of the variance of $\hat{e}$, which is not trivial to obtain specially for the QP and KSR mapping functions. It may be possible to compute the variance of $\hat{e}$ for those mapping functions by utilizing the bootstrapping method [23]. However, it is questionable whether the statistical query method would be necessarily more robust than the deterministic one with the QP and KSR mapping functions as with the OLS mapping function. Another factor to consider is the computational cost of implementing the bootstrapping method combined with the QP and KSR mapping functions, which are already computationally demanding.

B. Other Possible Mapping Functions

Designing a good mapping function is a challenging task mainly for two reasons. First, no prior knowledge about the appropriate form of the mapping function is available. Second, a mapping function suitable for certain hemodynamic features may not be the best choice for other hemodynamic features.

One alternative choice of mapping function is a feed-forward neural network (FFNW) since it is a flexible and versatile

method to approximate unknown functions. As pointed out in [14], however, it requires a large amount of data to properly train even a simple form of neural network such as a two-layer neural network. We may need hundreds of patients from whom we can collect ABP, CBFV, and ICP signals to train the two-layer neural network as the mapping function. The number of patients included in our current database is only 57, which makes the neural network mapping function an infeasible option. The FFNW mapping function may become affordable eventually when more patients are included in our database.

Another possible choice of a mapping function is a local linear fuzzy (LLF) mapping function. The LLF mapping function may be more versatile than other global mapping functions since the true mapping function between the hemodynamic features and dissimilarity measures is expected to be complex and heterogeneous. In addition, adopting the LLF mapping function may conform better to the local nature of the proposed data-mining framework, i.e., the final ICP simulation model is built upon *one* optimal database entry. One major concern to implement the LLF mapping function is its demanding computational load. However, it can be overcome by utilizing the parallel computing technique implemented on multicore processors.

C. Economical Considerations

With the burden of escalating cost of health care on our society, it is imperative to take economical implications into consideration when designing new test methods such as our endeavor in achieving noninvasive ICP assessment. The only existing ICP assessment technique in market is not only invasive but also uses single-usage sensors and catheters that cost about $500 on average. A screening test of high ICP that is widely used in clinic involves taking CT brain scans [24]–[26], which costs about $750–$1500. Compared with these costly techniques, an ultrasound based ICP assessment technique has inherent advantage as it can be repeatedly used without any disposable at fraction of cost ($150). The proposed data-mining framework works in theory with any other modalities of measuring ICP-related signals as a general calibration process for ICP values. Therefore, the choice of which related signal to use is a multifactorial decision problem where the economical implication should not be neglected.

Overall, our study results demonstrate that the performance of our data-mining framework for NICP assessment definitely improves by adopting a nonlinear mapping function such as the KSR technique instead of linear mapping functions both in the dissimilarity measure estimation and the mean ICP estimation. Given the component-wise nature of the data-mining framework, our future effort will continue to focus on improving other individual constituents of the framework to achieve a clinically viable noninvasive ICP assessment technique.

REFERENCES

[1] S. Aggarwal, D. Brooks, Y. Kang, P. Linden, and J. P. II, "Noninvasive monitoring of cerebral perfusion pressure in patients with acute liver failure using transcranial doppler ultrasonography," *Liver Transpl.*, vol. 14, pp. 1048–1057, 2008.

[2] F. S. Larsen, G. Strauss, G. M. Knudsen, T. M. Herzog, B. A. Hansen, and N. H. Secher, "Cerebral perfusion, cardiac output, and arterial pressure in patients with fluminant hepatic failure," *Crit. Care Med.*, vol. 28, pp. 996–1000, 2000.

[3] R. W. Sherman, R. A. Bowie, M. M. E. Henfrey, R. P. Mahajan, and D. Bogod, "Cerebral haemodynamics in pregnancy and pre-eclampsia as assessed by transcranial doppler ultrasonography," *Br. J. Anaesth.*, vol. 89, no. 5, pp. 687–692, Nov. 2002.

[4] O. Detry, A. D. Roover, P. Honoré, and M. Meurisse, "Brain edema and intracranial hypertension in fulminant hepatic failure: Pathophysiology and management," *World J. Gastroenterol.*, vol. 12, no. 46, pp. 7405–7412, Dec. 2006.

[5] O. Detry, N. Arkadopoulos, P. Ting, E. Kahaku, J. Margulies, W. Arnaout, S. D. Colquhoun, J. Rozga, and A. A. Demetriou, "Intracranial pressure during liver transplantation for fulminant hepatic failure1," *Transplantation*, vol. 67, no. 5, pp. 767–770, Mar. 1999.

[6] T. Ueno, B. R. Macias, W. T. Yost, and A. R. Hargens, "Noninvasive assessment of intracranial pressure waveforms by using pulsed phase lock loop technology. Technical note," *J. Neurosurg.*, vol. 103, no. 2, pp. 361–367, Aug. 2005.

[7] T. Ueno, R. E. Ballard, L. M. Shuer, J. H. Cantrell, W. T. Yost, and A. R. Hargens, "Noninvasive measurement of pulsatile intracranial pressure using ultrasound," *Acta Neurochir. Suppl.*, vol. 71, pp. 66–69, 1998.

[8] D. Michaeli and Z. H. Rappaport, "Tissue resonance analysis; a novel method for noninvasive monitoring of intracranial pressure. Technical note," *J. Neurosurg.*, vol. 96, no. 6, pp. 1132–1137, Jun. 2002.

[9] M. A. Belfort, C. Tooke-Miller, M. Varner, G. Saade, C. Grunewald, H. Nisell, and J. A. Herd, "Evaluation of a noninvasive transcranial doppler and blood pressure-based method for the assessment of cerebral perfusion pressure in pregnant women," *Hypertens. Pregnancy*, vol. 19, no. 3, pp. 331–340, 2000.

[10] M. Czosnyka, B. F. Matta, P. Smielewski, P. J. Kirkpatrick, and J. D. Pickard, "Cerebral perfusion pressure in head-injured patients: A noninvasive assessment using transcranial doppler ultrasonography," *J. Neurosurg.*, vol. 88, no. 5, pp. 802–808, May 1998.

[11] R. Aaslid, T. Lundar, K. Lindergaard, and H. Nornes, "Estimation of cerebral perfusion pressure from arterial blood pressure and transcranial doppler recordings," in *Proceedings Sixth International Symposium on Intracranial Pressure*, Glasgow, Scotland, 1985, J. D. Miller, G. M. Teasdale, J. O. Rowan, S. L. Galbraith, and A. D. Mendelow, Eds. New York: Springer-Verlag, 1986, pp. 226–229.

[12] B. Schmidt, M. Czosnyka, A. Raabe, H. Yahya, J. J. Schwarze, D. Sackerer, D. Sander, and J. Klingelhöfer, "Adaptive noninvasive assessment of intracranial pressure and cerebral autoregulation," *Stroke*, vol. 34, no. 1, pp. 84–89, Jan. 2003.

[13] B. Schmidt, M. Czosnyka, J. Schwarze, D. Sander, W. Gerstner, C. Lumenta, and J. Klingelhofer, "Evaluation of a method for noninvasive intracranial pressure assessment during infusion studies in patients with hydrocephalus," *J. Neurosurg.*, vol. 92, no. 5, pp. 793–800, 2000.

[14] X. Hu, V. Nenov, M. Bergsneider, and N. Martin, "A data mining framework of noninvasive intracranial pressure assessment," *Biomed. Signal Process. Control*, vol. 1, pp. 64–77, 2006.

[15] X. Hu, P. Xu, S. Wu, S. Asgari, and M. Bergsneider, "A data mining framework for time series estimation," *J. Biomed. Informat.*, vol. 43, no. 2, pp. 190–199, Apr. 2010.

[16] F. Zhang, Y. Q. Chen, and G. Bi, "Adaptive harmonic fractional fourier transform," in *Proc. IEEE Int. Symp. Circuits Syst.*, Geneva, May 2000, vol. 5, pp. 45–48.

[17] R. B. Panerai, S. L. Dawson, and J. F. Potter, "Linear and nonlinear analysis of human dynamic cerebral autoregulation," *Amer. J. Physiol.*, vol. 277, no. 3, pt. 2, pp. H1089–H1099, Sep. 1999.

[18] X. Hu and V. Nenov, "Multivariate AR modeling of electromyography for the classification of upper arm movements," *Clin. Neurophysiol.*, vol. 115, no. 6, pp. 1276–1287, 2004.

[19] J. Nocedal and S. J. Wright, *Numerical Optimization*, 2nd ed. New York: Springer-Verlag, 2006.

[20] D. Cai, X. He, and J. Han, "Efficient kernel discriminant analysis via spectral regression," Dept. Comput. Sci., Univ. Illinois, Urbana-ChampaignTech. Rep. UIUCDCS-R-2007-2888, Aug. 2007.

[21] F. Scalzo, S. Asgari, S. Kim, M. Bergsneider, and X. Hu, "Robust peak recognition in intracranial pressure signals," *Biomed. Eng. Online*, vol. 9, p. 61, Oct. 2010.

[22] S. Kim, M. Bergsneider, and X. Hu, "A systematic study of linear dynamic system modeling of intracranial pressure dynamics," *Physiol. Meas.*, vol. 32, no. 3, pp. 319–336, 2011.

[23] B. Efron and R. Tibshirani, *An Introduction to the Bootstrap*. New York: Chapman & Hall, 1993.

[24] K. E. Saatman, A.-C. Duhaime, R. Bullock, A. I. Maas, A. Valadka, and G. T. Manley, "Classification of traumatic brain injury for targeted therapies," *J. Neurotrauma*, vol. 25, no. 7, pp. 719–738, Jul. 2008.

[25] A. Maas, C. Hukkelhoven, L. Marshall, and E. Steyerberg, "Prediction of outcome in traumatic brain injury with computed tomographic characteristics: A comparison between the computed tomographic classification and combinations of computed tomographic predictors," *Neurosurgery*, vol. 57, no. 6, pp. 1173–1182, Dec. 2005.

[26] L. F. Marshall, S. B. Marshall, M. R. Klauber, M. Van Berkum Clark, H. Eisenberg, J. A. Jane, T. G. Luerssen, A. Marmarou, and M. A. Foulkes, "The diagnosis of head injury requires a classification based on computed axial tomography," *J. Neurotrauma*, vol. 9 (Suppl. 1), pp. S287–292, Mar. 1992.

Authors' photographs and biographies not available at the time of publication.